High-resolution in situ hybridization analysis on the chromosomal interval 61C7-61C8 of Drosophila melanogaster reveals interbands as open chromatin domains

Zielke, T., Glotov, A., Saumweber, H.

This is the final version of the manuscript. The original article has been published as Online First publication on 31 October 2015 and in final edited form in:

Chromosoma
2016 JUNE ; 125(3): 423-435
Springer Verlag

The final publication is available at Springer via: http://dx.doi.org/10.1007/s00412-015-0554-5

High resolution *in situ* hybridization analysis on the chromosomal interval 61C7-61C8 of *Drosophila melanogaster* reveals interbands as open chromatin domains.

Thomas Zielke*, Alexander Glotov* and Harald Saumweber[a]

Institute of Biology, Cytogenetics Group, Humboldt University Berlin, Germany

Chausseestr. 117, 10115 Berlin, Germany

Key words: histone modifications, insulators, boundaries, polytene chromosomes

*both authors contributed equally to this work

[a] to whom correspondence should be addressed

Author for correspondence:

Prof. Dr. H. Saumweber
Humboldt Universität zu Berlin
Institut für Biologie - Zytogenetik
Chausseestr. 117
10115 Berlin

hsaumweber@gmail.com
tel.: -49-30-20938178
fax.: -49-30-20938177

Abstract

Eukaryotic chromatin is organized in contiguous domains that differ in protein binding, histone modifications, transcriptional activity and in their degree of compaction. Genome-wide comparisons suggest that overall the chromatin organization is similar in different cells within an organism. Here we compare the structure and activity of the 61C7-61C8 interval in polytene and diploid cells of *Drosophila*. By *in situ* hybridization on polytene chromosomes combined with high resolution microscopy we mapped the boundaries of the 61C7-8 interband and of the 61C7 and C8 band regions respectively. Our results demonstrate that the 61C7-8 interband is significantly larger than estimated previously. This interband extends over 20 kbp and is in the range of the flanking band domains. It contains several active genes and therefore can be considered as an open chromatin domain. Comparing the 61C7-8 structure of *Drosophila* S2 cells and polytene salivary gland cells by ChIP for chromatin protein binding and histone modifications, we observe a highly consistent domain structure for the proximal 13 kbp of the domain in both cell types. However, the distal 7 kbp of the open domain differ in protein binding and histone modification between both tissues. The domain contains four protein coding genes in the proximal part and 2 noncoding transcripts in the distal part. The differential transcriptional activity of one of the noncoding transcripts correlates with the observed differences in the chromatin structure between both tissues. The significance of our findings for the organization and structure of open chromatin domains will be discussed.

53 **Introduction**

54

55 Interphase chromosomes are organized as a series of cis-acting domains that differ in gene density,
56 transcriptional activity and degree of compaction and may form units for dynamic 3D nuclear folding.
57 Although such a chromosomal domain organization was consistently found by different approaches,
58 we are only beginning to understand the details of domain architecture, boundary formation,
59 domain establishment and dynamic maintenance. Powerful genome-wide approaches correlating
60 gene density and activity with features of chromatin analyzed by means of high-performance
61 bioinformatic methods (Sexton et al. 2012; Van Bortle and Corces 2012; Schwartz et al. 2012; Van
62 Bortle et al. 2014; Matzat and Lei 2014; Zhimulev et al. 2014) widened our view and strongly
63 supported the formulation of different concepts, although a breakthrough in understanding domain
64 formation and function still lies ahead.

65 Early on, chromatin research in diptera, foremost *Drosophila*, had an enormous influence on our
66 views on chromosomal domain organization. Polytene interphase chromosomes due to chromatid
67 amplification and restricted 3D folding represent a formidable example for such a cis-organization of
68 domains. Microscopic preparations of such chromosomes reveal an organized and reproducible
69 pattern of compacted chromomeres (bands) interrupted by less compacted interband domains
70 (Painter 1934; Beermann 1972). The difference in chromatin compaction was established by
71 cytophotometry (Beermann 1972) and EM dry mass determination (Laird 1980). RNA labeling and
72 RNA-polymerase localization *in situ* suggest, that interbands in contrast to bands are the
73 transcriptionally active part of the genome (Alcover et al. 1981; Alcover et al. 1982; Jammrich et al.
74 1977). This view was challenged by the limited coding capacity of interbands estimated to represent
75 only ~5% of the total genome (Beermann 1972; however compare Laird 1980) and by the
76 observation, that many of the RNA-polymerase molecules found in interbands are not
77 transcriptionally engaged but are in a paused state (Weeks et al. 1998). Therefore, interbands were
78 proposed to contain only regulatory elements that form a functional unit with the gene body located
79 in the adjacent bands. In fact, a situation reflecting this model was found by high resolution
80 cytogenetic analysis which demonstrated that an important regulatory region of the *Notch* gene
81 (Welshons and Keppy 1975), containing several alternative promoters (Vasquez and Schedl 2000)
82 was located in the 3C6-7 interband and the Notch gene body was fully included in the adjacent band
83 3C7. Later studies from the Zhimulev group (Demakov et al. 2004; Zhimulev et al. 2014)
84 complemented this view by demonstrating that other interbands may contain ubiquitously expressed
85 genes.

86 Together with the chromosomal domain concept the issue of domain boundaries came up. The first
87 domain boundaries described were located at the flanks of the *Drosophila* hsp70 domain. They are
88 formed by the scs and scs´ DNA elements and essentially require the binding of the Zw(5) and BEAF-
89 32 DNA binding proteins respectively for their function (Gaszner et al. 1999; Zhao et al. 1995). Zw(5)
90 and BEAF-32 spatially interact and fold the DNA containing the two hsp70A genes and two genes of
91 unknown function into a chromatin loop (Blanton et al. 2003) consistent with a model of genome
92 wide looped domain formation proposed by Benyajati and Worcel (1976). Moreover, BEAF-32 bound
93 to scs´ shows insulator properties, protecting from inappropriate enhancer activity, consistent with
94 its proposed boundary function (Zhao et al. 1995). Meanwhile other chromatin proteins with
95 insulator properties were identified in *Drosophila*, that either bind DNA elements (BEAF-32, dCTCF,

96 GAGA-factor, TFIIIC, Su(Hw), Zw(5)) or associate with one of the primary DNA bound insulators
97 (CP190, Topors, Mod(mdg4)) and some of these proteins (CTCF, TFIIIC) are conserved in vertebrates
98 (Vogelmann et al. 2011; Schwartz et al. 2012; Van Bortle and Corces 2012; Matzat and Lei 2014).
99 Genome wide analysis identified thousands of binding sites for most of these proteins (Bushey et al.
100 2009; Schwartz et al. 2012; Van Bortle et al. 2014). Recent evidence suggests diverse functions for
101 these proteins and only a subset of sites forming dense clusters of protein binding at domain borders
102 may provide true boundary function (Matzat and Lei 2014; Van Bortle et al. 2014).

103 Studies of Sexton and coworkers (2012) confirmed the existence of contiguous chromosomal
104 domains along eukaryotic chromosomes. On the other hand, genome wide chromatin data were also
105 used to create combinatorial maps (color codes) that revealed similar contiguous chromatin domains
106 with discrete properties. Filion and colleagues (2010) used DamID profiling data for 53 chromatin
107 proteins from *Drosophila* Kc167 cells to obtain five principal chromatin types defined by unique
108 combinations of proteins. The chromatin type "blue", marked by polycomb group protein binding
109 and the chromatin type "green" enriched for HP1 and associated proteins were classified as two
110 distinct forms of heterochromatin. The repressive "black" chromatin is relatively gene poor and is
111 marked by SUUR, Su(Hw) and Lamin binding. Finally, two distinct euchromatic chromatin types, the
112 yellow and red chromatin show properties of transcriptionally active chromatin and substantial
113 amounts of mRNA and RNA polymerase binding. Kharchenko and coworkers (2011) used genome
114 wide ChIP data of chromatin protein binding, DNaseI hypersensitivity and genomic run-on sequence
115 reads in S2 and BG3 cells to establish a nine color code that was in many aspects similar to the 5-
116 state model of Filion and colleagues (2010). Their states 1-5 (red, purple, brown, coral and green)
117 largely overlap the red and yellow chromatin of the Filion 5-state model. State 6 (dark grey) matches
118 with the 5-state blue chromatin, stage 7 (dark blue) and 8 (light blue) match with green and stage 9
119 (light grey) often coincides with black chromatin of the 5-state model. Typically for both models,
120 stretches of active chromatin alternate with extended domains of different forms of inactive
121 chromatin. Combining cytogenetic data with chromatin color coding, and a variety of genomic data
122 on active and inactive chromatin marks, the Zhimulev group found a good correspondence between
123 the cytogenetic band/interband structure of selected regions of polytene chromosomes with
124 characteristic features of inactive/active chromatin from the same regions of S2 cells respectively
125 (Vatolina et al. 2011; Demakov et al. 2011). Extending these studies a four state chromatin model
126 was established based on the presence/absence of 12 interband specific proteins that was tested at
127 32 interband loci mapped by EM data (Zhimulev et al. 2014). They found that chromatin, that was
128 bound by all 12 interband specific proteins (cyan chromatin) correlated with all of their 32 mapped
129 interband locations and therefore should be typical for interband chromatin. Furthermore blue
130 chromatin, that contained less RNA polymerase and no Chriz protein was associated with so called
131 grey bands. The green and magenta chromatin type was not further specified, but correlated with
132 less active condensed chromatin regions.

133 As a model for testing mechanisms of open chromatin domain formation we selected the 61C7-8
134 interband (Zielke and Saumweber 2014), one of the best studied interbands that was also mapped by
135 EM analysis (Semeshin et al. 1989; Demakov et al. 1993; Demakov et al. 2004; Semeshin et al. 2008;
136 Berkaeva et al. 2009). In the present paper we report the cytogenetic mapping of the 61C7 to 61C8
137 region including the 61C7-8 by high resolution *in situ* hybridization. We find that this interband is
138 significantly larger than previously reported. Similar to the adjacent interband 61C8-9 it contains
139 several genes that are actively transcribed in diploid and polytene cells and it has a DNA content
140 comparable with the flanking 61C7 and 61C8 bands, that both have a lower gene density and gene

activity. Thus, the 61C7-8 interband forms an active open chromatin domain, a property that might be shared by many other interband domains.

Results

Mapping the chromatin region 61C7-8 on polytene chromosomes by high resolution FISH

Previous EM work by Semeshin and coworkers (1989) mapped a P-element insertion (*P[hsp70:Adh](61C)*) that generated a new band 61C7´ within the 61C7-8 interband. Using DNA probes from the inserted P-element Demakov and colleagues (1993) isolated genomic DNA from the flanking 61C7-8 interband region. In order to map the full extent and the boundaries of the 61C7-8 interband we used this information to design a series of 21 genomic 1 kbp fragments as *in situ* probes to start a chromosomal walk over the chromosomal interval 61C7 to C8 including the 61C7-8 interband (see fig.1).

As a first approximation for positioning the probes we oriented ourselves to data from S2 cells for the pattern of histone modifications, the insulator proteins BEAF-32, CTCF and CP190 and the chromatin proteins Chriz and Jil-1 in the region of interest (fig. 1 and Online Resource 1; data from modENCODE; Gan et al., 2011; Gortchakov et al., 2005; Zielke and Saumweber 2014). Initially, we assumed H3K27me3 to mark condensed (band) chromatin whereas histone modifications H3K4me3, H3K4me2, H3K9ac as well as BEAF-32-, CP190-, Jil-1- and Chriz- binding would mark open (interband) chromatin and its boundaries respectively (Van Bortle et al., 2014; Zhimulev et al., 2014). The precise genomic coordinates of the hybridization probes are given in table 1.

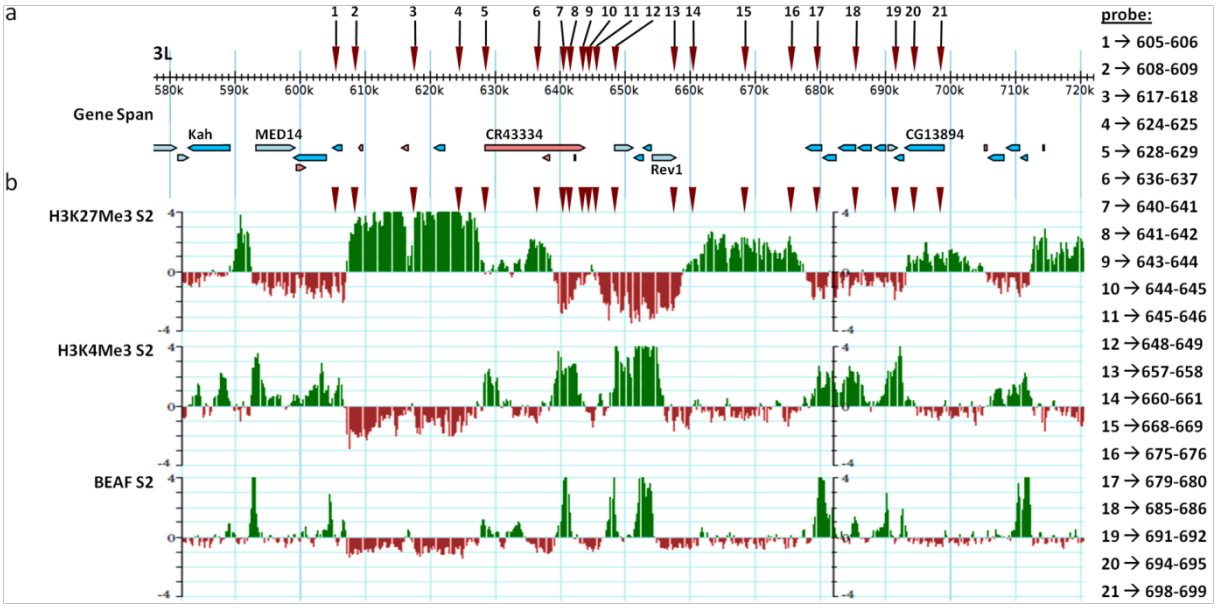

Fig 1.: Chromosomal walk for high resolution *in situ* hybridization analysis of the 61C7-61C8 region: a) molecular coordinates of the chromosomal interval under investigation along with genes mapping in this region. b) shows ChIP profiles of top: H3K27me3, middle H3K4mMe3 and bottom BEAF-32 mapped for this region on *Drosophila* S2-cell chromatin (above zero line in green and below zero line in red enrichment and depletion of histone modification/protein binding respectively displayed as log SD; data from modENCODE (http://modencode.oicr.on.ca/fgb2/gbrowse/fly/). Brown arrowheads in a and b indicate the location of the 1kbp genomic DNA probes used for *in situ* analysis. Probe numbers were given in a distal to proximal orientation whereby distal is towards the tip of 3L. The genomic coordinates for 21 *in situ* probes in kbp are given at the right side of the figure.

Table 1: molecular and cytogenetic location of hybridization probes used for mapping 61C7-8

probe No.[1]	molecular coordinates (kbp)	cytogenetic location	Genes mapping in the cytogenetic interval of the corresponding band or interband respectively[2]		
			Gene name	function	coordinates 3L (kbp)
1	605-606	interband 61C6-7	n.a.	n.a.	n.a.
2	608-609	interband/band boundary 61C7	n.a.	n.a.	n.a.
3	617-618	band 61C7	*CG43337*	n.n.	620.7-622.3
4	624-625	band 61C7	*CR44513*	non-coding; n.n.	609.2-609.6
5	628-629	band 61C7	*CR42719*	non-coding; n.n.	615.6-616.6
6	636-637	band 61C7	*CR43334*[3]	non-coding; n.n.	628.4-643.9
			CR43423	non-coding; n.n.	637.5-638.6
7	640-641	band/interband boundary 61C7	n.a.	n.a.	n.a.
8	641-642	interband 61C7-8			
9	643-644	interband 61C7-8	*CG12030/*	UDP-Galactose-	648.6-651.3
10	644-645	interband 61C7-8	*Gale*	4´-epimerase	
11	645-646	interband 61C7-8	*CG3402*	n.n.	651.5-652.9
12	648-649	interband 61C7-8	*MED30*	Mediator	653.0-654.1
12a[4]	650-654[4]	interband 61C7-8[4]		complex subunit	
13	657-658	interband 61C7-8	*Rev1*	DNA repair	648.6-651.3
			bantam	miRNA	642.208-288
			CR43334-RB[4]	non-coding; n.n.	639.7-642.3
14	660-661	interband/band boundary 61C8	n.a.	n.a.	n.a.
15	668-669	band 61C8	none	none	none
16	675-676	band 61C8			
17	679-680	band/interband boundary 61C9	n.a.	n.a.	n.a.
18	685-680	interb. 61C8-C9/D1[5]	*RabX6*	GTPase	690.5-691.9
19	691-692	interb. 61C8-C9/D1[5]	*CG17129*	n.n.	677.9-680.3
20	694-695	interb. 61C8-C9/D1[5]	*CG3386*	MADF domain	680.4–682.0
21	698-699	interb. 61C8-C9/D1[5]	*earthbound 1*	DNA-binding	682.9-685.5
			CG3344	put. peptidase	685.9-688.0
			CG32483	put. peptidase	688.5-690.1
			Vti1	put. vSNARE	691.5-692.9
			CG13894	put. DNA-binding	693.1-699.1

[1] probes numbered from distal to proximal (bp), abbreviations: n.a. not applicable; n.n. unknown
[2] data from FlyBase/ modENCODE (http://modencode.oicr.on.ca/fgb2/gbrowse/fly/)
[3] *CR43334* encodes three alternate transcripts A,B,C. CR43334-RB initiates at the distal boundary of 61C7-8.
[4] data from Zielke and Saumweber (2014)
[5] band 61C9 reported by Bridges (1941) was not detectable at EM resolution (Semeshin et al. 1989)

For each probe at least 3 independent *in situ* hybridization experiments were performed. On average for each probe 5 chromosomes with a distinct signal in the region of interest were recorded. Some of the *in situ* results for representative probes that were critical for the determination of the boundaries of the 61C7-8 interband are shown in figure 2. From these data, a preliminary allocation of the *in situ* probes to bands, interbands or boundaries could be obtained (table1). For instance, probe 605-606 is located in the interband 61C6-7, distal to band 61C7, probe 624-625 is within the 61C7 band, probe

648-649 is within the interband 61C7-8 and probe 691-692 locates to the interband 61C8-C9/D1 (see below). The full set of representative images of each *in situ* probe of the chromosomal walk is presented in Online Resource 2.

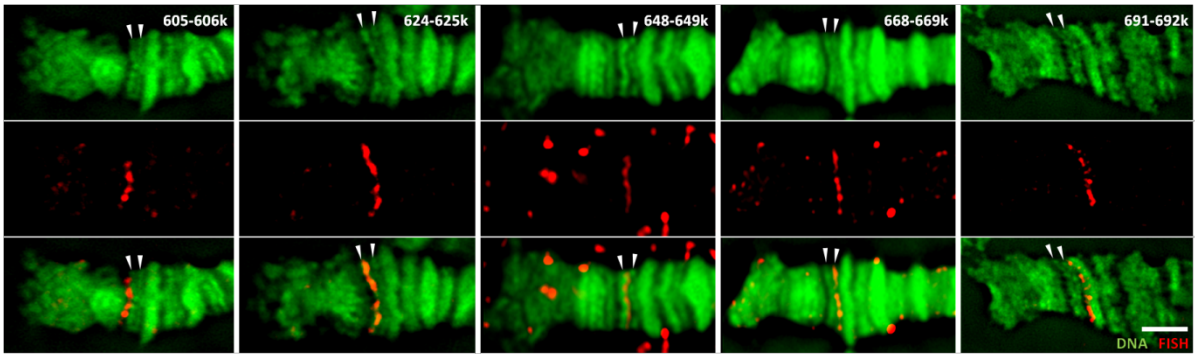

Figure 2. Representative *in situ* hybridization probes mapping to the 61C7-8 region. Panels show successive *in situ* hybridization in the 61C7-8 region with representative 1 kbp probes from distal to proximal 3L with the genomic coordinates of the probes indicated as given in table 1. Top in each panel DNA staining (green), middle: *in situ* hybridization signal (red), bottom: merge. White arrowheads indicate the bands at 61C7 and 61C8 respectively. Distal to the left. Bar 3 μm.

Since the images were acquired by DeltaVision image restoration microscopy they retain information of the recorded fluorescence intensity and therefore allow quantitative evaluation of intensity profiles across the recorded signals. We used this feature to precisely determine the position of each probe as the center of the recorded signal (for details see Methods). The relative cytogenetic position of each probe, as the value of the mean, was plotted against the genomic position in kbp. The resulting line profile for the full image data set is shown in figure 3c. In the graph the slope is proportional to the ratio of relative cytological distance to the length of DNA, therefore proportional to chromatin compaction. A steep slope (a large relative distance traversed per kbp) indicates decompacted chromatin, whereas a flat slope is expected for compacted chromatin (a small relative distance traversed per kbp). As evident from figure 3c, the slopes of the graph and therefore the degree of compaction, change in a predictable way. Regions allocated by previous visual inspection to interbands show a steep slope indicating decondensed chromatin. In contrast, regions previously allocated to bands show a flat slope as expected for more condensed chromatin. Interestingly, we observed a sudden change in the slope at several positions within a ~2-3 kbp genomic interval, as would be expected at the boundaries between domains differing in their degree of condensation. We therefore suggest that these regions indicate the position of the boundaries between condensed (band) and decondensed (interband) chromatin domains as was proposed for the 3C6-7 interband by Rykowski and coworkers (1988; see discussion).

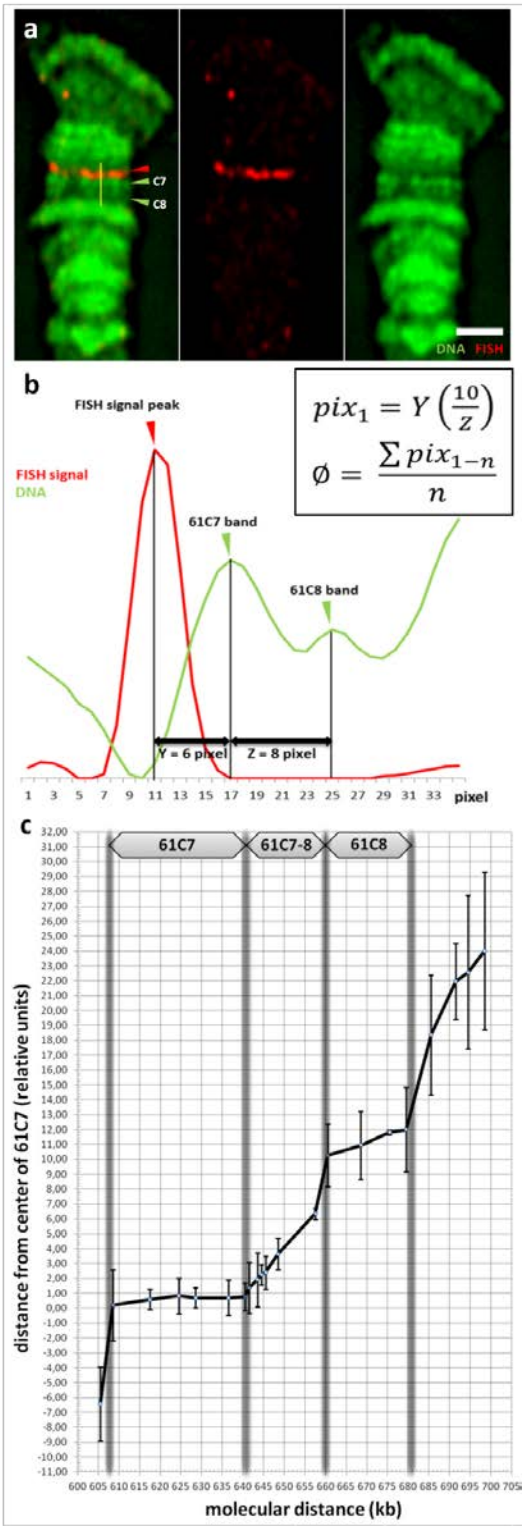

Figure 3. High resolution mapping of chromatin domains and boundaries in the 61C7-61C8 region: a) DNA staining (green), *in situ* hybridization (red) and a merged image is shown for a representative data set used to determine the cytogenetic position of the given *in situ* signal on the distal 3L chromosome. The yellow bar indicates position of the line scans shown in (b). The position of the bands 61C7 and 61C8 is indicated by arrowheads. b) Line scan of DNA-staining (green) and *in situ* hybridization signal (red) in the 61C7-8 region of the 3L chromosome along the yellow line displayed in (a). The determination of the distance Y for the *in situ* signal to the reference band 61C7 and for the distance Z between the reference band 61C7 and the band 61C8 used to normalize data is indicated. The equation for the calculation of the relative cytogenetic distance in pixel

226 ($pix_i=Y_i(10/Z_i)$) and for the calculation of the average value ($Ø = \sum pix_{1-n}/n$) for each probe is further specified in
227 the methods section. c) graphic representation of the relative cytogenetic distance of the *in situ* probes plotted
228 against the absolute distance of the same probes on genomic DNA in kbp. Note, that the slope in the graph
229 represents the degree of condensation and is inversely correlated to the degree of condensation. The
230 boundaries of the domains 61C7, 61C7-8 and 61C8 are defined by positions of abrupt changes in the slope with
231 an estimated precision of 2-3 kbp (details see text).

232 Taking the data from the graph in figure 3c, we place the 61C7-8 open chromatin domain between
233 the coordinates 3L: 640-660±2 kbp (fig. 4, Online Resource 1 and table 1). The 20 kbp domain
234 contains four protein coding genes in its proximal part. In addition, two noncoding genes are located
235 in the distal part of the domain. The bulk of *CR43334,* a large noncoding gene with unknown
236 function, localizes within 61C7. It encodes three alternate transcripts that are transcribed in proximal
237 direction. One of them, CR43334-RB, initiates at the distal boundary of the 61C7-8 domain and
238 overlaps the *bantam* gene, an 80 nt miRNA transcribed on the same strand.

239 According to the criteria mentioned we also mapped the extent of the adjacent condensed domains
240 61C7 and 61C8 (fig. 4, Online Resource 1 and table 1). The distally located band 61C7 extends over 30
241 kbp DNA (3L: 608-640±2 kb) and contains one coding and four noncoding genes. *CR43334* already
242 mentioned before is mainly located within 61C7. However, CR43334-RB, one of its three alternate
243 transcripts, starts at the distal end of the 61C7-8 interband. The proximal condensed band domain
244 61C8 (3L: 660–680±2 kbp) contains 20 kbp DNA and is therefore smaller than 61C7. This is reflected
245 by a comparatively weaker DNA signal for 61C8 (see fig. 2). In addition, due to its comparatively
246 steeper slope (fig. 3c), 61C8 may be less condensed than 61C7. There are no transcripts mapped to
247 this domain.

248

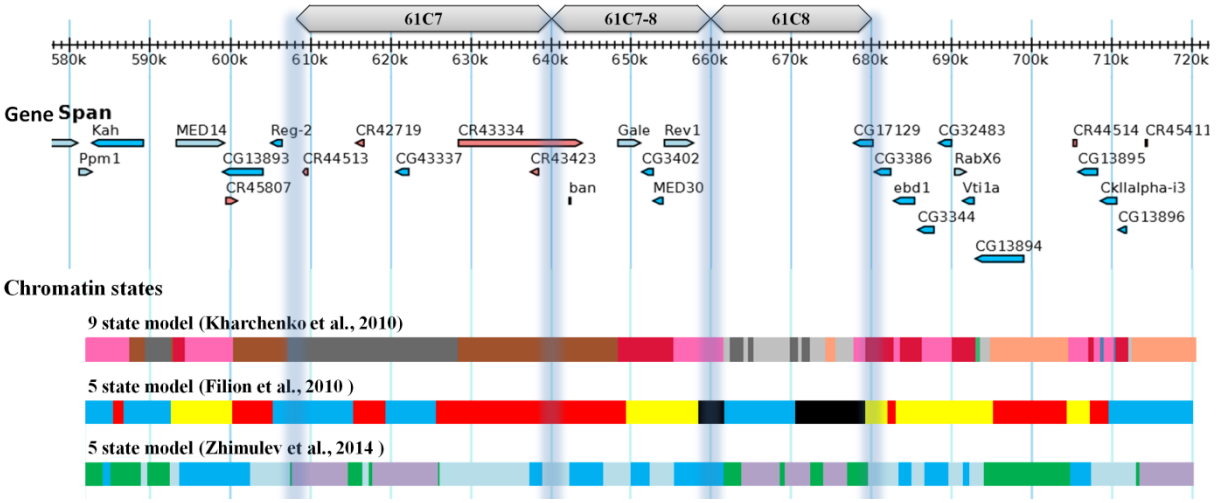

249

250 **Figure 4. Chromatin domains, boundaries and chromatin states in the 61C7-8 interval:** top: Genomic
251 coordinates of the interval investigated; grey bars indicate extent of mapped domains; middle: coding (blue,
252 light blue) and noncoding (brown) genes mapped in this region, data from flybase/modENCODE
253 (http://modencode.oicr.on.ca/fgb2/gbrowse/fly/); bottom: chromatin states presenting by color coding as
254 published previously by Kharchenko et al. (2011), Filion et al. (2010) and Zhimulev et al. 2014. Vertical blue
255 shaded bars indicate location of boundaries (± 1kbp) mapped by our *in situ* approach.
256

257 A decondensed region that we assign to the 61C8-C9/D1 interband follows immediately proximal to
258 61C8 forming an open domain with a size of minimally 20 kbp. The designation of the distal boundary
259 as C9/D1 was chosen since the C9 band originally mapped by Bridges (1941) could not be confirmed

by EM analysis (Semeshin et al. 1989). Regardless, the boundary to the 61C9/D1 interband domain is proximal to our most proximal probe 21 (698–699 kbp). The mapped section of the C61C8-C9/D1 open chromatin domain is densely packed with eight coding genes that are transcribed in distal direction with the exception of *RabX6* (fig. 4, Online Resource 1 and table 1). The interband region immediate distal of 61C7 is also densely packed with coding genes. However, its distal boundary was not further mapped by the current study.

Known interband chromatin proteins are located within the 61C7-8 domain

Data for genome wide binding of many interband specific proteins in Drosophila S2 cells are available (flybase/modENCODE (http://modencode.oicr.on.ca/fgb2/gbrowse/fly). In S2 cells, BEAF-32, Chriz, Jil-1 and CP190 were found at many sites that were mapped as open chromatin by their pattern of histone modifications, nucleosome density, DNase I hypersensitivity and susceptibility for transgene insertion (Vatolina et al. 2011, Zhimulev et al. 2014). The interband domains mapped by our *in situ* walk on salivary gland chromosomes coincide with such open regions mapped in S2 cells (fig. 4; Online Resource 1). Assuming that the epigenetic state is conserved between both cell types we would expect to observe the binding of these proteins within the mapped cytogenetic interval.

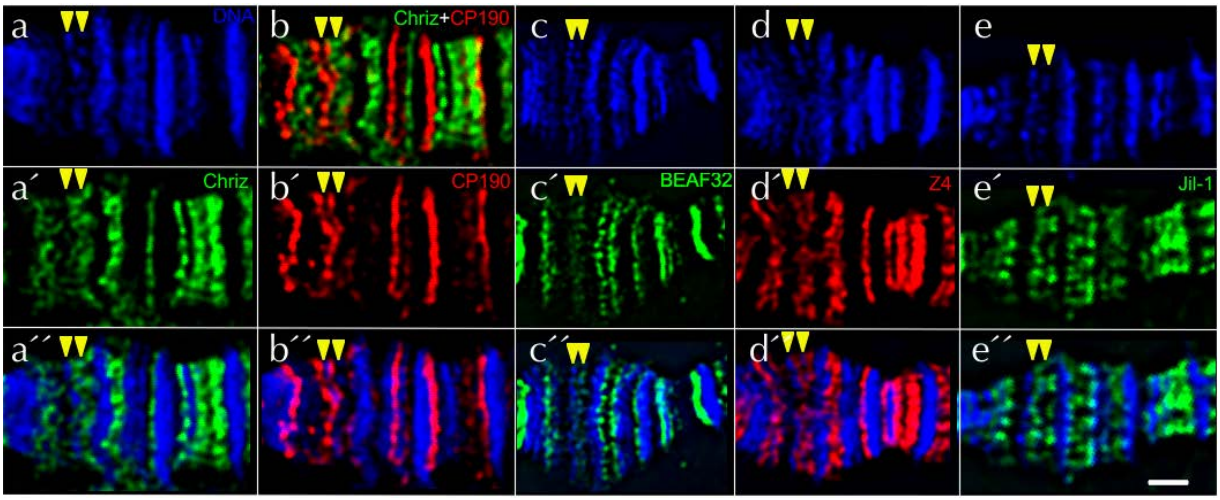

Figure 5. Chromatin protein binding in the 61C7-8 region: Indirect immunofluorescence was performed on single and double stained, formaldehyde fixed salivary gland polytene chromosomes. a-a´´) DNA blue; Chriz staining green; merge of Chriz with DNA; b-b´´) double staining (same chromosome as in a-a´´) b) merge of Chriz green and CP190 red; b´)CP190 red; b´´ merge of CP190 with DNA; c-c´´) DNA blue; BEAF-32 staining green; merge of BEAF-32 with DNA; d-d´´) DNA blue; Z4 staining red; merge of Z4 with DNA; e-e´´) DNA blue; Jil-1 staining green; merge of Jil-1 with DNA; distal left; the position of the more distal band 61C7 and the proximal 61C8 band is labelled by yellow arrowheads throughout; note that the 61C7-8 interband shows a signal for all tested proteins; bar 2μm.

We therefore analyzed the binding of BEAF-32, CP190, Chriz, Jil-1 and Z4 to polytene salivary gland chromosomes by indirect immunofluorescence (fig. 5). All proteins are bound in the 61C7-8 open domain as expected. In the 61C6-7 interband all proteins are detectable, though weakly, except CP190 that shows a prominent signal. Furthermore, all proteins bind within the 61C8-C9/D1 open domain. At the condensed domains 61C7 and 61C8 no binding of any of these proteins is observed. This is not a limitation of our staining method, since we can clearly localize histones and other non-histone proteins at these sites (data not shown).

Protein binding and histone modifications differ in the distal part of 61C7-8 between S2 cell and salivary gland cell chromatin

To probe chromatin protein binding at higher resolution we used ChIP/qPCR thereby concentrating mainly to the 61C7-8 open domain (fig. 6). A comparison of ChIP data for the Chriz binding on S2 cell chromatin obtained from modENCODE and our own experiments shows identical results, confirming that our ChIP method is reliable. In S2 cells ChIP reveals that Chriz is bound in three broad regions in the 61C7-8 interband: distally a smaller peak between 640-642 kbp followed by a prominent binding region between 647-650 kbp and a double-peak region at 652-655 kbp (fig. 6 b, c). Interestingly, in salivary gland cell chromatin the distal Chriz peak at 640-642 kbp is not formed (fig. 6d).

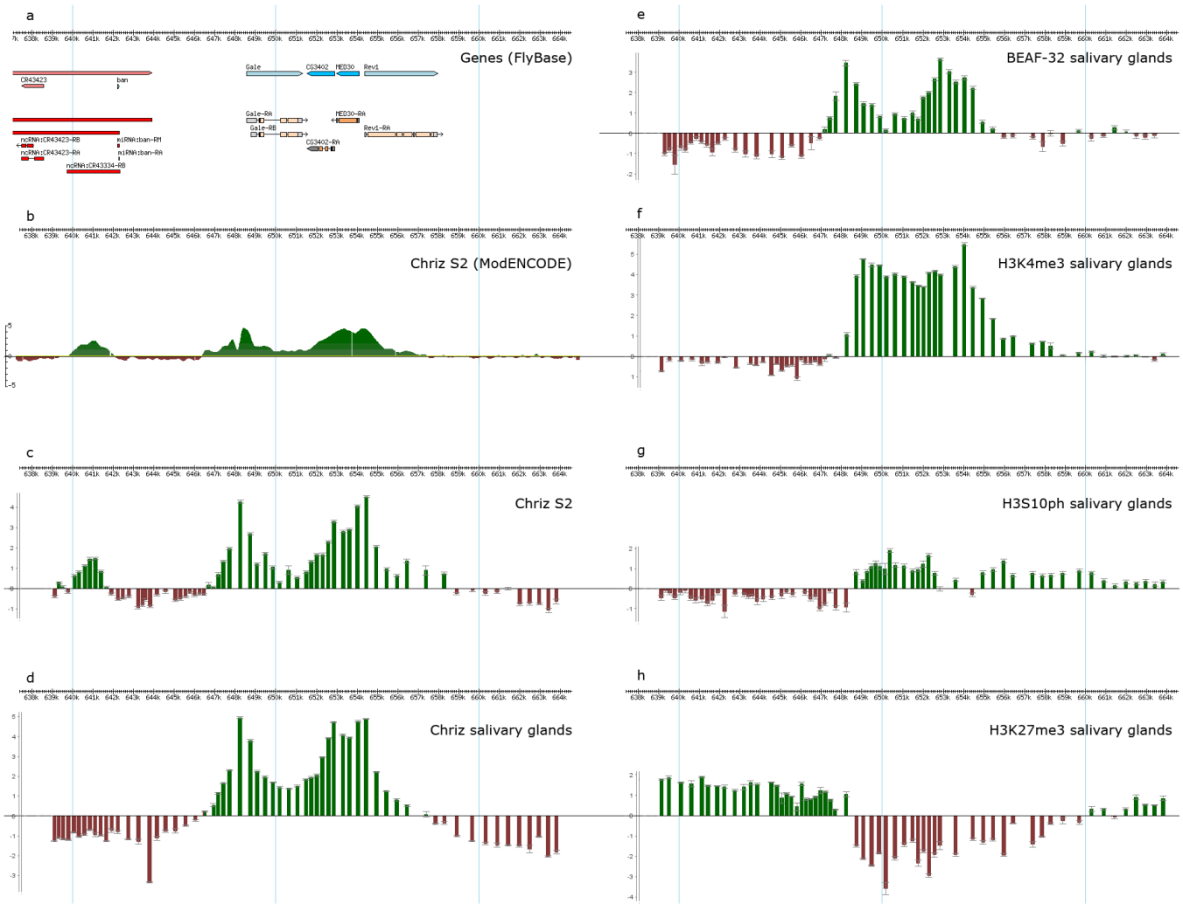

Figure 6. Comparison of the Chromatin state of the 61C7-8 open domain in diploid and polytene cells: ChIP/qPCR was performed on S2 cell and salivary gland chromatin and data for the 61C7-8 open chromatin domain were plotted against genomic coordinates of distal 3L; a) location of genes in the region of interest; b) ChIP profile for Chriz (flybase/modENCODE (http://modencode.oicr.on.ca/fgb2/gbrowse/fly) binding in S2 cells; c) ChIP profile for Chriz binding in S2 cells (own data); d) ChIP profile for Chriz binding in salivary gland cells; note the absence of the distal peak of Chriz binding; e) ChIP profile for BEAF-32 binding in salivary gland cells; f) ChIP profile for H3K4me3 histone modification in salivary gland cells; g) ChIP profile for H3S10ph histone modification in salivary gland cells; h) ChIP profile for H3K27me3 histone modification in salivary gland cells. Values plotted above zero line in green and below zero line in red indicate enrichment/depletion of histone modification/protein binding respectively as log SD. Error bars represent deviation between three technical replicas in one of two biological samples.

316 In S2 cells BEAF-32 shows four binding peaks in the 61C7-8 in open domain: at 640-642 kbp, 647-649
317 kbp and 652-654 kbp partially overlapping a peak at 655 kbp (Online Resource 1). However, similarly
318 to Chriz binding, the distal BEAF peak at 640-642 kbp is not detectable in ChIPs from salivary gland
319 cell chromatin (fig. 6e). In the remaining part of the 61C7-8 domain the binding of BEAF-32 and Chriz
320 in salivary glands is indistinguishable from their binding in S2 cells.

321 Similarly, in the distal region the chromatin modifications present on S2 cell chromatin differed from
322 those detected on salivary gland cell chromatin. In S2 cells H3K27me3 is depleted in the whole 61C7-
323 8 open domain (639-659 kbp; Online Resource 1). In contrast, in salivary gland cell chromatin
324 H3K27me3 modification spreads into the distal part of the domain up to position 648 kbp, restricting
325 the H3K27me3 depleted zone to 649-659 kbp (fig. 6f). On the opposite, H3K4me3, a mark for
326 transcriptionally active open chromatin, that is found in the S2 cells between the coordinates 639-
327 656 kbp (Online Resource 1) is restricted in salivary gland cells to the proximal part of the domain,
328 between 648-656 kbp (fig. 6g). H3S10ph in salivary glands is detected between the coordinates 648-
329 660 kbp. This corresponds well to the distribution of the Jil-1 kinase in salivary gland chromatin
330 (Online Resource 3; see Cai et al. 2014), which is the enzyme responsible for this modification in
331 interphase. Unfortunately, there are no data for H3S10ph distribution in S2 interphase cells.
332 However, Jil-1 kinase binds between the coordinates 639-642 kbp in S2 cells (Online Resource 3; see
333 Cai et al. 2014).

334

335 **The transcriptional state of noncoding gene *CR43334* in the distal part of 61C7-8 differs between S2**
336 **cells and salivary gland cells**

337 To figure out whether the observed difference in the chromatin structure between S2 cells and
338 salivary gland cells in distal part of 61C7-8 comes along with different transcriptional state in the
339 genes located in this part of the domain, we compared the transcription within this interval by RT-

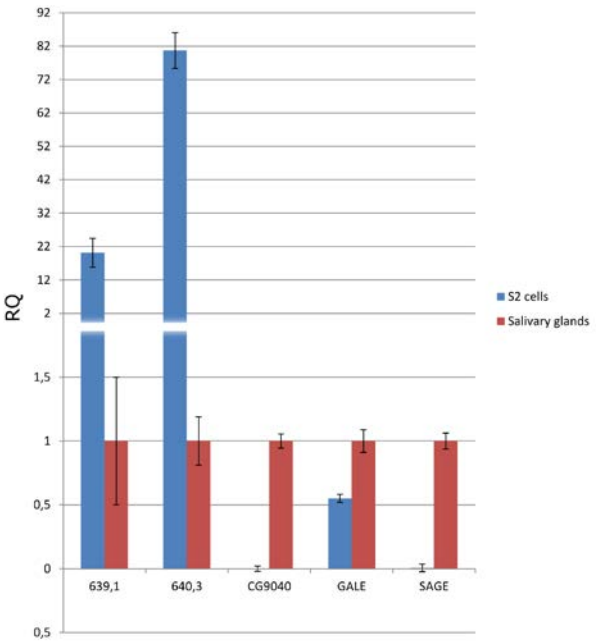

340

341 **Figure 7. Transcription of genes in the 61C7-8 domain in S2 cells and salivary gland cells:** Total RNA isolated
342 from salivary glands or S2 cells was investigated by qRT-PCR using primer pairs within the noncoding transcripts
343 CR43334-RA (639,1) and CR43334-RB (640,3). Two salivary gland specific genes (*CG9040* and *Sage*) and *Gale*

344 were taken as a control. The expression values were normalized relative to *Actin42a* (1.0) and plotted as
345 relative fold change (RQ) on the abscissa for each primer pair side by side for expression in S2 cells (blue) and
346 salivary glands (red). Error bars represent deviation between three technical replicas of two biological samples.

347

348 qPCR of total RNA isolated from both sources. (fig. 7). The coding genes in the proximal region were
349 transcribed in both tissues to similar rates except *CG12030/Gale* that was ~3-fold higher expressed in
350 salivary glands (Online Resource 4). Interestingly, qRT-PCR with primer pairs specific for the CR43334-
351 RB transcript in the distal part of 61C7-8 showed, that this transcript was robustly expressed in S2
352 cells but not in salivary glands (fig. 7).

353

354 **Discussion**

355 We determined the cytogenetic domain boundaries within the 61C7-8 interval on polytene
356 chromosomes by high resolution *in situ* hybridization. The method uses state of the art FISH
357 protocols combined with quantitative microscopy based on iterative deconvolution, a combination
358 that was previously successfully applied for mapping the boundaries of the 3C6-7 interband on the X-
359 chromosome (Rykowski et al. 1988). The algorithm of deconvolution used in this method allows
360 quantitative sampling of the signal by including the out of focus information of the fluorescence
361 emission from the probe. Peak intensity measurements for the DNA and the *in situ* signals were used
362 for the precise determination of probe position relative to the position of a reference band nearby.
363 Normalization of the distances was possible by using a second reference band on the same
364 chromosome to control for local stretching. Combining data from several chromosomes on the same
365 or on different slides, we obtained reliable mean values for relative distance between the probe and
366 reference band. The reliability of the method was already critically discussed by Rykowski and
367 coworkers (1988). Depending on the density and the length of our hybridization probes we could
368 determine the domain boundaries with a precision of 2-3 kbp. Within ~70 kbp these boundaries
369 define three distinct chromosomal domains including the 30 kbp 61C7 and 20 kbp 61C8 condensed
370 band domains and the 20 kbp 61C7-8 open interband domain. In addition, the adjacent 61C8-C9/D1
371 (at least 18 kbp) and 61C6-7 open domains were partially mapped.

372 The domains differ in their degree of condensation but do not significantly differ in their DNA
373 content. According to our data the 61C7-8 interband is larger than previously estimated (Demakov et
374 al. 1993; Semeshin et al. 2008). It extends over ~20kbp and contains four coding and two noncoding
375 genes. Therefore, it is approximately of the same size as the flanking condensed band domains 61C7
376 and 61C8 that were estimated to contain 30 and 20 kbp respectively. Although we did not yet map
377 the boundary position of 61C9/D1 band, we estimate the adjacent interband 61C8-C9/D1 to include
378 at least 20 kbp and nine protein coding genes. Within the mapped interval open domains contain a
379 moderate to high number of protein coding genes, whereas the condensed band domains have a
380 significantly lower gene density and contain more noncoding genes. From the data of the relative
381 length/kbp ratio displayed in fig. 3 we estimate, that the chromatin in the band 61C7 is ~10x and of
382 the band 61C8 ~5x more condensed than the 61C7-8 interband chromatin. Considering our
383 provisional data on the minimal extent of the interband 61C8-C9/D1 we arrive at similar estimates.
384 Therefore, we feel it justified to define both interbands as distinct open chromatin domains
385 harboring several genes.

386 Our observation that the 61C7-8 interband forms an open chromatin domain is corroborated by the
387 binding of interband specific proteins to this domain, as observed by immunostaining. The proteins
388 Chriz, Z4, Jil-1, BEAF-32 and CP190 are localized in this region as well as in the adjacent distal and
389 proximal interbands. Available ChIP data for S2 cells suggest a distinct binding of these proteins to
390 the mapped 61C7-8 open domain with four peaks (642, 648.5, 653 and 654kbp) for BEAF-32 and
391 Chriz, and two peaks (648.5 and 654 kbp) for CP190. Jil-1 shows a rather broad binding between 648-
392 662 (binding data for Z4 are not available). To our surprise, the distalmost 642 kbp peak of BEAF-32-
393 and Chriz-binding was not observed in salivary gland chromatin, although this chromatin section
394 clearly belongs to the open domain according to our *in situ* mapping. An independent argument that
395 this DNA belongs to the open chromatin domain is provided by the work of Demakov and colleagues
396 (1993). This element is 2 kbp proximal of the P-element insertion at 3L: 639.7 kbp that was used as a
397 starting point for cloning the adjacent 61C7-8 interband DNA (Demakov et al. 1993). Considering
398 histone modifications we also note differences between S2 and salivary gland cells in the fine
399 structure of the distal 61C7-8 domain. Initially, the depletion of H3K27me3 (639-659kbp) and the
400 enrichment of H3K4me3 (639-656 kbp) were considered as useful marks for open chromatin. Both
401 enrichment for H3K4me3- and depletion for H3K27me3-chromatin in S2 cells correspond well with
402 the extent of the open domain mapped by our *in situ* approach (640-660 kbp). Surprisingly, this was
403 not the case for salivary gland cell chromatin. Here H3K4me3-enrichment and H3K27me3-depletion
404 are restricted to the proximal part of the domain (H3K4me3-enrichment: 649-659 kbp; H3K27me3-
405 depletion: 648-660 kbp). We therefore conclude, that the open state of the distal part of the 61C7-8
406 domain as mapped by our *in situ* approach does not depend on these two modifications, making it
407 less likely, that they are directly involved in the formation of the distal boundary of 61C7-8.

408 However, this does not exclude a role of protein binding and histone modifications in the formation
409 of chromatin structure of proximal 61C7-8. There, the Chriz protein may be recruited by specific
410 interaction with DNA binding proteins like BEAF-32 (Vogelmann et al. 2014). Chriz may recruit H3S10
411 kinase Jil-1 whose enzyme activity has the potential for local opening of condensed chromatin (Deng
412 et al., 2008). Furthermore, the zinc-finger protein Z4, a specific interactor of Chriz (Gortchakov et al.
413 2005; Gan et al. 2011) was reported to recruit the *Drosophila* NURF chromatin remodeling complex
414 required for open chromatin formation of active genes (Kugler and Nagel 2010; Kugler et al. 2011).
415 The reported dependency of the distinct polytene chromosome structure on the presence of Chriz,
416 Z4 and Jil-1 (Eggert et al. 2004; Rath et al. 2006) as well as the requirement of Z4 for proliferation and
417 growth (Kugler and Nagel 2007) is consistent with these observations

418 Open domain formation may be correlated with transcription related processes, like promoter
419 activity, paused transcripts or transcription elongation. For instance the open state of the proximal
420 61C7-8 domain coincides with the four coding genes actively transcribed in the region. In particular
421 *CG12030/Gale* is strongly expressed in both tissues (Online Resource 4). Similarly, the adjacent
422 interband 61C8-C9/D1 contains a number of genes that are moderately transcribed in salivary glands
423 and therefore its open state is correlated with transcription activity as well (Online Resource 4). Of
424 note, the mere presence of promoters and upstream regulatory sequences was described as a
425 sufficient condition for interband formation. The ~800 bp N^{fswb} deletion results in the loss of 3C6-7
426 interband (Welshons and Keppy 1975). This fragment was mapped to the 1.5 kbp 3C6-7 interband
427 (Rykowski et al. 1988). It contains several of the alternative *Notch* promoters and upstream DNase
428 hypersensitive sites (Vasquez and Schedl 2000) and is not transcribed in salivary glands. A 274 bp
429 subfragment from this region can induce transcription independent open domain formation at an
430 ectopic position (Andreenkov et al. 2012). A 4.7 kbp fragment (637.6-642.3) from the distal boundary

431 of the 61C7-8 domain was also reported to induce open chromatin ectopically within putative silent
432 chromatin (Semeshin et al. 2008). However, it may not be autonomous in this function. In their
433 experiments Semeshin and coworkers (2008) inserted the 4.7 kbp fragment in opposite orientation
434 650 bp upstream of a functional hsp70 promoter element. Hsp70 is known to be active even at
435 ambient temperature and therefore may contribute to local decondensation. In a somewhat
436 different chromatin setting, a 5 kbp DNA fragment from 61C7-8 fully including the 4.7 kbp element
437 failed to induce open chromatin ectopically (Zielke and Saumweber 2014). In these experiments no
438 additional promoter elements were present. However, the 5 kbp 61C7-8 fragment encodes a 2.6 kbp
439 alternate CR43334-RB transcript that is expressed in S2 cells but not in salivary glands. Its promoter
440 sequences (INI and DPE) as well as several putative binding sites for the transcription factor ADF-1
441 are located at 639.6-639.8 at the distal boundary of the 61C7-8 open domain and DNA fragments
442 overlapping these elements were shown to possess enhancer properties (Berkaeva et al. 2009). The
443 expression of CR43334-RB in S2 cells may coincide with the increased H3K4me3- and depleted
444 H3K27me3-modification and with Chriz and BEAF-32 binding in the distal 61C7-8 domain. In salivary
445 glands the absence of CR23334-RB expression may result in altered histone modifications and
446 protein binding in distal 61C7-8. However, this does not affect the formation of open chromatin in
447 this region, as demonstrated by our *in situ* mapping results. The CR43334 promoter elements and the
448 transcription factor binding sites, in cooperation with the proximal acting factors, may still keep this
449 chromatin in an open conformation.
450
451 Several genomic chromatin profiling data sets were used previously to establish color code maps of
452 *Drosophila* chromatin domains that differ in structure and function (Filion et al. 2010; Kharchenko et
453 al. 2011; Zhimulev et al. 2014). Although these maps are based on data from diploid *Drosophila* cell
454 lines related to embryonic hemocyte- (S2) or neural- (Kc) lineages, they fit very well to the
455 boundaries and the condensation state of the domains mapped by our *in situ* approach (fig 4). The
456 suggestion that the domain structure is conserved in different tissues is certainly true for the distal
457 boundary of 61C7 and 61C8 as well as for the proximal boundary of the 61C8 band. The
458 cytogenetically mapped boundaries coincide with transitions between repressed and active
459 chromatin states for all three color code schemes. Moreover, proximal of 61C8, distal of 61C7 and for
460 the 61C7-8 section all color code maps indicate active chromatin states consistent with the open
461 interband domain structure mapped by our approach. Although the color coding maps provide less
462 evidence, ChIP data for histone modifications and protein binding in S2 cells clearly indicate a
463 chromatin transition at 640 kbp (online resource 1). We therefore suggest that the proximal
464 boundary of 61C7 mapped by our *in situ* approach that coincides with changes in chromatin structure
465 of S2 cells represents the default state of chromatin folding in both cell types.
466
467 Color codes typical for active chromatin in principle match our open domains but are based on data
468 that were obtained at much higher resolution. The more details they include, the more mosaic the
469 color pattern becomes within a domain determined by cytogenetic methods. Even in the five color
470 code of Filion and colleagues (2010), the cytogenetically mapped domains are not of uniform color.
471 Not unexpectedly, this suggests that cytogenetic domains form integral units of slightly different
472 chromatin states that reflect the underlying activity of genes and regulatory sequences which they
473 contain. Zhimulev and coworkers (2014) used a combination of cytogenetic EM mapping and color
474 coding based on interband protein binding to allocate DNA sections to cytogenetically mapped
475 chromosomal domains. They proposed that chromatin classified “cyan” represents interbands and
476 classified “blue” chromatin may correspond to “grey” bands. In their algorithm the two states differ

477 mainly by the presence of the Chriz protein that often exhibits a very restricted local binding.
478 Although we do not want to exclude that in some cases this distinction may be valid, it cannot be
479 general. Our data clearly demonstrate that the 61C7-8 interband is composed of two peripheral and
480 one central sections of "blue" separated by two sections of "cyan" chromatin (fig. 4). A contribution
481 of "blue" and "cyan" chromatin to one and the same interband is also suggested for the interbands
482 immediately distal and proximal of 61C6 or 61C7 respectively.
483
484 To our knowledge our approach provides the best resolution we currently can obtain in cytogenetic
485 analysis of chromatin to match microscopic with molecular data. Our data strongly support
486 conclusions from correlation studies, that the boundaries and architecture of physical contiguous
487 domains (Sexton et al. 2012) are largely shared between diploid and polytene cells of different origin
488 (Vatolina et al. 2012; Demakov et al. 2012; Zhimulev et al. 2014). This adds to the long standing
489 assumption that cytogenetically defined chromatin domains on polytene chromosomes are
490 conserved in interphase cells. Organization and dynamics of contiguous chromatin domains have
491 important functions in the control of proliferation, growth and differentiation of cells and tissues.
492 Knowing the boundaries and the extent of chromatin domains will allow us to predict sequence
493 elements and mechanisms regulating their properties. Based on this knowledge, methods that
494 introduce site specific modifications of essential sequences within domains and boundaries can be
495 devised (Zielke and Saumweber, 2014; Hsu et al., 2014) that will be instrumental for better
496 understanding of domain functions.
497
498 **Materials and methods**

499 Fluorescence *in situ* hybridization (FISH) and determination of the relative position of the FISH signal
500
501 1 kbp DNA templates for the labeling reaction were prepared by PCR on genomic DNA from *Oregon R*
502 flies. The sequences of the primers used are available on request. The biotin-labeled 1 kbp DNA
503 probes were prepared by treatment of the purified PCR-products with BNT-Mix (Roche) according to
504 the manufacturer's protocol. The labeled DNA-probes were used for *in situ* hybridization as described
505 by Langer-Safer and coworkers (1982). For microscopy, a DeltaVision Spectris Optical Sectioning
506 Microscope (OSM) equipped with 60x and 100x lenses, a polychroic beamsplitter suitable for DAPI
507 and RD-TR-PE and filter sets DAPI (EX360/40; EM457/50) and RD-TR-PE (EX555/28; EM617/73) was
508 used. Images were obtained as a stack of optical sections that were deconvolved using DeltaVision
509 SoftWorx software. Single sections from the center of the stack were used for the analysis of signal
510 intensity profiles.
511
512 From the selected section a line scan of the FISH *in situ* signal as well as the DNA (DAPI) signal was
513 recorded along a representative line spanning the mapped chromosomal region (fig. 3a). We used
514 this line scan to precisely determine the position of the center of the probe as the pixel with the
515 maximum intensity value across the *in situ* hybridization signal. Similarly, the positions of the 61C7
516 and 61C8 bands were determined from the same profile as the maximum intensity values measured
517 across the DNA (DAPI) signals. The pixel distance pix_i between the maximum of the FISH signal peak
518 and the maximum of the 61C7 DNA reference band peak (Y_i) was normalized to the distance (Z_i)
519 between 61C7 to 61C8. To compensate for differences in local stretching between the chromosomes,
520 the equation $pix_i=Y_i(10/Z_i)$ was applied (fig. 3b). In this way, on the average five chromosomes from
521 three different slides were evaluated and used for the calculation of the mean of the distance value

522 (Ø) for each probe (equation $Ø = \sum pix_{1-n}/n$ in fig. 3b and Online Resource 5). Then, the relative
523 cytogenetic position for each probe was plotted against the genomic position in kbp (fig. 3c).
524

525 Immunostaining
526
527 Polytene chromosomes were prepared from third-instar larvae and immunostaining was performed
528 as described by Eggert and coworkers (2004). All polyclonal antisera were obtained from Biogenes
529 (Berlin) following immunization with affinity purified proteins expressed in *E. coli* by our laboratory.
530 Primary antibodies against the following proteins were used: BEAF-32 (rabbit, 1:1000), Chriz (rabbit,
531 1:1000), CP190 (mouse monoclonal Bx63, 10 mg/ml), Jil1 (rabbit, 1:1000), Z4 (rabbit, 1:1000). As
532 secondary antibodies we used: Alexa-Fluor-488- or -555-conjugated goat anti-mouse-IgG or anti-
533 rabbit-IgG antibodies (Invitrogen) at 1:1000 dilution. Microscopy was as described for FISH.
534

535 ChIP

536 The primer pairs for ChIP were designed to amplify 180-200 bp fragments covering the 639-664 kbp
537 region of 3L chromosome. The sequences of the primers are available on request. Chromatin
538 immunoprecipitation was performed according to the protocol of Legube et al. (2006). Chromatin
539 was prepared either from 10^7 S2 cells or 100 pairs of L3 salivary glands. The following antibodies
540 were used: anti-Chriz rabbit polyclonal (own production, animal 6177), anti-BEAF-32 rabbit
541 polyclonal (own production, animal 21352), anti-H3S10Ph (ab14955, Abcam), anti-H3K4me3 (ab8580,
542 Abcam), anti-H3K27me3 (39155, Active Motif). To reverse crosslinks the immunoprecipitated DNA
543 was incubated at 65˚C overnight, treated with RNAse A and purified using Chip DNA Clean &
544 Concentrator Kit (Zymo research, D5205). Relative quantification analysis has been used to
545 determine fold enrichment over mock control. For estimation of ChIP efficiency of our own antisera,
546 enrichment over input was calculated for two probes positioned at 652,9 kbp and 654,2 kbp. With
547 BEAF32 antisera 14,6±0,8 and 7,7±0,7 percent of input DNA was precipitated for respective tested
548 sites. ChIP with Chriz antisera for the same sites resulted in precipitation of 27,7±2,0 and 24,7±1,3 %
549 of input, respectively.

550

551 RNA expression analysis

552 RNA for expression analysis was isolated from 20 pairs of third-instar larvae salivary glands or 10^7 S2
553 cells using Quick-RNA MiniPrep Kit (Zymo Research, R1054). cDNA synthesis was performed using
554 Oligo dT/Random hexamer primer mixture and RevertAid Premium Reverse Transcriptase (Thermo
555 Scientific) following the manufacturer's protocol. Actin42a was used as the endogenous control in
556 further qPCR analysis.

557

558 Real-time PCR analysis

559 Quantitative PCR of ChIP and expression analysis was performed using SYBR Green PCR master mix
560 (Applied Biosystem) in a StepOnePlus Real-Time PCR system (Applied Biosystem). The amplification

561 parameters were as follows: 10 min at 95°C, 40 cycles of 15 s at 95°C followed by 1 min at 60°C. At
562 the end of the program the melting curve was recorded.

563 **Acknowledgements**

564 We thank Petra Binting and Irina Passow for excellent technical assistance.

565

566 **Funding** This work was supported by a grant of the Deutsche Forschungsgemeinschaft,
567 SA338/12-1 given to H.S.
568
569
570 **Conflict of interest** The authors declare that they have no conflict of interest.
571
572
573 **Ethical approval** All applicable international, national, and institutional guidelines for the care
574 and use of animals were followed. This article does not contain any studies with human participants
575 performed by any of the authors.
576

577 **References**

578 Alcover A, Izquierdo M, Stollar BD, Miranda M, Alonso C (1981) Analytical studies of chromosomal
579 transcription detected by an endogenous hybridization technique (EHT) using autoradiography and
580 indirect immunofluorescence in *Drosophila* hydei. Acta Embryol Morphol Exp. 2:131-140.

581 Alcover A, Izquierdo M, Stollar BD, Kitagawa Y, Miranda M, Alonso C (1982) In situ
582 immunofluorescent visualization of chromosomal transcripts in polytene chromosomes.
583 Chromosoma 87:263-277.

584 Andreenkov OV, Volkova EI, Semeshin, VF, Zhimulev IF, Demakov SA (2013) Structural Features of
585 3C6/C7 Interband Chromatin Organization in *Drosophila* melanogaster Polytene Chromosomes. Cell
586 and Tissue Biology 7:347–351.

587 Beermann W (1972) Chromomeres and genes. In: Beermann W, Reinert J and Ursprung H (eds)
588 Results and Problems in Cell Differentiation: 4. Developmental Studies on Giant Chromosomes,
589 Springer Berlin, pp.1-34

590 Benyajati C, Worcel A (1976) Isolation, characterization, and structure of the folded interphase
591 genome of *Drosophila* melanogaster. Cell 9:393-407.

592 Berkaeva M, Demakov S, Schwartz YB, Zhimulev IF (2009) Functional analysis of *Drosophila* polytene
593 chromosomes decompacted unit: the interband. Chrom Res 17:745-757.

594 Blanton J, Gaszner M, Schedl, P (2003) Protein:protein interactions and the pairing of boundary
595 elements in vivo. Genes Dev 17:664-675.

596 Bridges PN (1941) A revised map of the left limb of the third chromosome of *Drosophila*
597 melanogaster. J Hered 32:64-66.

598 Bushey AM, Ramos E, Corces, VG (2009) Three subclasses of a *Drosophila* insulator show distinct and
599 cell type-specific genomic distributions. Genes Dev 23:1338-1350.

600 Cai W, Wang C, Li Y, Yao C, Shen L, Liu S, Bao X, Schnable PS, Girton J, Johansen J, Johansen KM
601 (2014) Genome-wide analysis of regulation of gene expression and H3K9me2 distribution by JIL-1
602 kinase mediated histone H3S10 phosphorylation in *Drosophila*. Nucl Ac Res 42:5456-5467.

603 Demakov SA, Semeshin VF, Zhimulev, IF (1993) Cloning and molecular genetic analysis of *Drosophila*
604 melanogaster interband DNA. Mol Gen Genet 238:437-443.

605 Demakov S, Gortchakov A, Schwartz Y, Semeshin V, Campuzano S, Modolell J, Zhimulev I (2004)
606 Molecular and genetic organization of *Drosophila* melanogaster polytene chromosomes: evidence for
607 two types of interband regions. Genetica 122:311-324.

608 Demakov SA, Vatolina TY, Babanko VN, Semeshin VF, Belyaeva ES, Zhimulev IF (2011) Protein
609 composition of interband regions in polytene and cell line chromosomes of *Drosophila* melanogaster.
610 BMC Genom 12:566-578.

611 Deng H, Bao X, Cai W, Blacketer MJ, Belmont AS, Girton J, Johansen J, Johansen KM (2008) Ectopic
612 histone H3S10 phosphorylation causes chromatin structure remodeling in *Drosophila*. Development
613 135:699-705.

614 Eggert H, Gortchakov A, Saumweber H (2004) Identification of the *Drosophila* interband-specific
615 protein Z4 as a DNA-binding zinc-finger protein determining chromosomal structure. J Cell Sci
616 117:4253-4264.

617 Filion GJ, van Bemmel JG, Braunschweig U, Talhout W, Kind J, Ward LD, Brugman W, de Castro IJ,
618 Kerkhoven RM, Bussemaker HJ, van Stensel B (2010) Systematic protein location mapping reveals five
619 principal chromatin types in *Drosophila* cells. Cell 143:212-224.

620 Gan M, Moebus S, Eggert H, Saumweber H (2011) The Chriz-Z4 complex recruits JIL-1 to polytene
621 chromosomes, a requirement for interband specific phosphorylation of H3S10. J Biosci 36: 425-438.

622 Gaszner M, Vazquez J, Schedl P (1999) The Zw5 protein, a component of the scs chromatin domain
623 boundary, is able to block enhancer -promoter interaction. Genes Dev 13:2098-2107.

624 Gortchakov AA, Eggert H, Gan M, Mattow J, Zhimulev IF, Saumweber H (2005) Chriz, a
625 chromodomain protein specific for the interbands of *Drosophila melanogaster* polytene
626 chromosomes. Chromosoma 114:54-66.

627 Hsu PD, Lander ES, Zhang F (2014) Development and application of CRISPR-Cas9 for genomic
628 engineering. Cell 157:1262-1278.

629 Jamrich MJ, Greenleaf AL, Bautz, EKF (1977) Localization of RNA polymerase in polytene
630 chromosomes of *Drosophila melanogaster*. Proc Natl Acad Sci USA 74:2079-2083.

631 Kharchenko PV, Alekseyenko AA, Schwartz YB, Minoda A, Riddle NC, Ernst J, Sabo PJ, Larschan E,
632 Gortchakov AA, Gu T, Linder-Basso D, Plachetka A, Shanower G, Tolstorukov MY, Luquette LJ, Xi R,
633 Jung YL, Park RW, Bishop EP, Canfield TK, Sandstorm R, Thurman RE, MacAlpine DM,
634 Stamatoyannopoulos JA, Kellis M, Elgin SCR, Kuroda M, Pirrotta V, Karpen GH, Park PJ (2011)

635 Comprehensive analysis of the chromatin landscape in *Drosophila melanogaster.* Nature 471:480-
636 485.

637 Kugler SJ, Nagel AC (2007) *putzig* Is Required for Cell Proliferation and Regulates Notch Activity in
638 *Drosophila*. Mol Biol Cell 18:3733–3740

639 Kugler SJ, Nagel AC (2010) A Novel Pzg-NURF Complex Regulates *Notch* Target Gene Activity. Mol Biol
640 Cell 21:3443-3448.

641 Kugler SJ, Gehring EM, Wallkamm V, Krüger V, Nagel AC (2011) The Putzig-NURF Nucleosome
642 Remodeling Complex Is Required for Ecdysone Receptor Signaling and Innate Immunity in *Drosophila*
643 *melanogaster*. Genetics 188:127–139.

644 Laird, CD (1980) Structural paradox of polytene chromosomes. Cell 22:869-874.

645 Langer-Safer PR, Levine M, Ward DC (1982) Immunological method for mapping genes on *Drosophila*
646 polytene chromosomes.Proc. NatL Acad. Sci. USA 79:4381-4385.

647 Legube G, McWeeney SK, Lercher MJ, Akhtar A (2006) X-chromosome-wide profiling of MSL-1
648 distribution and dosage compensation in *Drosophila*. Genes Dev 20:871-883.

649 Mazat LH, Lei EP (2014) Surviving an identity crisis: A revised view of chromatin insulators in the
650 genomics era. Biochim Biophys Acta. 1839:203-214.

651 Painter TS (1934) Salivary chromosomes and the attack on the gene. J Hered 25:465-476.

652 Rath U, Ding Y, Deng H, Qi H, Bao X, Zhang W, Girton J, Johansen J, Johansen, KM (2006) The
653 chromodomain protein, Chromator, interacts with JIL-1 kinase and regulates the structure of
654 *Drosophila* polytene chromosomes. J Cell Sci 119:2332-2341.

655 Rykowski MC, Parmelee SJ, Agard, DA, Sedat JW (1988) Precise determination of the molecular limits
656 of a polytene chromosome band: regulatory sequences for the *Notch* gene are in the interband. Cell
657 54:461-472.

658 Schwartz YB, Linder-Basso D, Kharchenko PV, Tolstorukov MY, Kim M, Li H-B, Gorchakov AA, Minoda
659 A, Shanower G, Alekseyenko AA, Riddle NC, Jung YL, Gu T, Plachetka A, Elgin SCR, Kuroda MI, Park PJ,
660 Savitsky M, Karpen GH, Pirrotta V (2012) Nature and function of insulator protein binding sites in the
661 *Drosophila* genome. Genome Research 22:2188–2198.

662 Semeshin, VF, Demakov SA, Perez Alonso M, Belyaeva ES, Bonner JJ, Zhimulev IF (1989) Electron
663 microscopical analysis of *Drosophila* polytene chromosomes. V. Characteristics of structures formed
664 by transposed DNA segments of mobile elements. Chromosoma 97:396-412.

665 Semeshin VF, Demakov SA, Shloma VV, Vatolina TY, Gorchakov AA, Zhimulev, IF (2008) Interbands
666 behave as decompacted autonomous units in *Drosophila melanogaster* polytene chromosomes.
667 Genetica 132:267-279.

668 Sexton, T, Yaffe E, Kenigsberg E, Bantignies F, Leblanc B, Hoichman M, Parrinello H, Tanay A, Cavalli G
669 (2012) Three-dimensional folding and functional organization principles of the *Drosophila* genome.
670 Cell 148:458-472.

671 Van Bortle K, Corces VG (2012) Nuclear organization and genome function. Annu Rev Cell Dev Biol
672 28:163-187.

673 Van Bortle K, Nichols MH, Li L, Ong C-T, Takenaka N, Qin ZS, Corces VG (2014) Insulator function and
674 topological domain border strength scale with architectural protein occupancy. Genome Biology
675 15:R82.

676 Vazquez J, Schedl P (1994) Sequences required for enhancer blocking activity of scs are located
677 within two nuclease-hypersensitive regions. EMBO J. 13:5984-5993.

678 Vasquez J, Schedl P (2000) Deletion of an insulator element by the mutation *facet-strawberry* in
679 *Drosophila melanogaster*. Genetics 155:1297-1311.

680 Vatolina TY, Boldyreva LV, Demakova OV, Demakov SA, Kokoza EB, Semeshin VF, Babenko VN,
681 Goncharov FP, Belyaeva ES, Zhimulev IF (2011) Identical functional organization of nonpolytene and
682 polytene chromosomes in *Drosophila melanogaster*. PLoS ONE 6(10): e25960.

683 Vogelmann J, Valeri A, Guillou E, Cuvier O, Nöllmann M (2011) Roles of chromatin insulator proteins
684 in higher order chromatin organization and transcription regulation. Nucleus 2:358-369.

685 Vogelmann J, Le Gall A, Dejardin S, Allemand F, Gamot A, Labesse G, Cuvier O, Nègre N, Cohen-
686 Gonsaud M, Margeat E, Nöllmann M (2014) Chromatin insulator factors involved in long-range DNA
687 interactions and their role in the folding of the *Drosophila* genome. PLoS Genet 10(8):e1004544.

688 Weeks JR, Hardin SE, Shen J, Lee JM, Greenleaf AL (1993) Locus specific variation in phosphorylation
689 state of RNA polymerase II in vivo: correlations with gene activity and transcript processing. Genes
690 Dev 7:2329-2344.

691 Welshons WJ, Keppy, DO (1975) Intragenic deletions and salivary band relationships in *Drosophila*.
692 Genetics 80:143-155.

693 Zhimulev IF, Zykova TY, Goncharov FP, Khoroshko VA, Demakova OV, Semeshin VF, Pokholkova GV,
694 Boldyreva LV, Demidova DS, Babenko VN, Demakov SA, Belyaeva E (2014) Genetic organization of
695 interphase chromosome bands and interbands in *Drosophila melanogaster*. PLoS ONE 9(7): e101631.

696 Zhao K, Hart CM, Laemmli UK (1995) Visualization of chromosomal domains with boundary element-
697 associated factor BEAF-32. Cell 81:879-889.

698 Zielke T, Saumweber H (2014) Dissection of open chromatin domain formation by site-specific
699 recombination in *Drosophila*. J Cell Science (2014) 127:2365–2375.
700

Online Resource Materials

Online Resource 1 (ESM1)

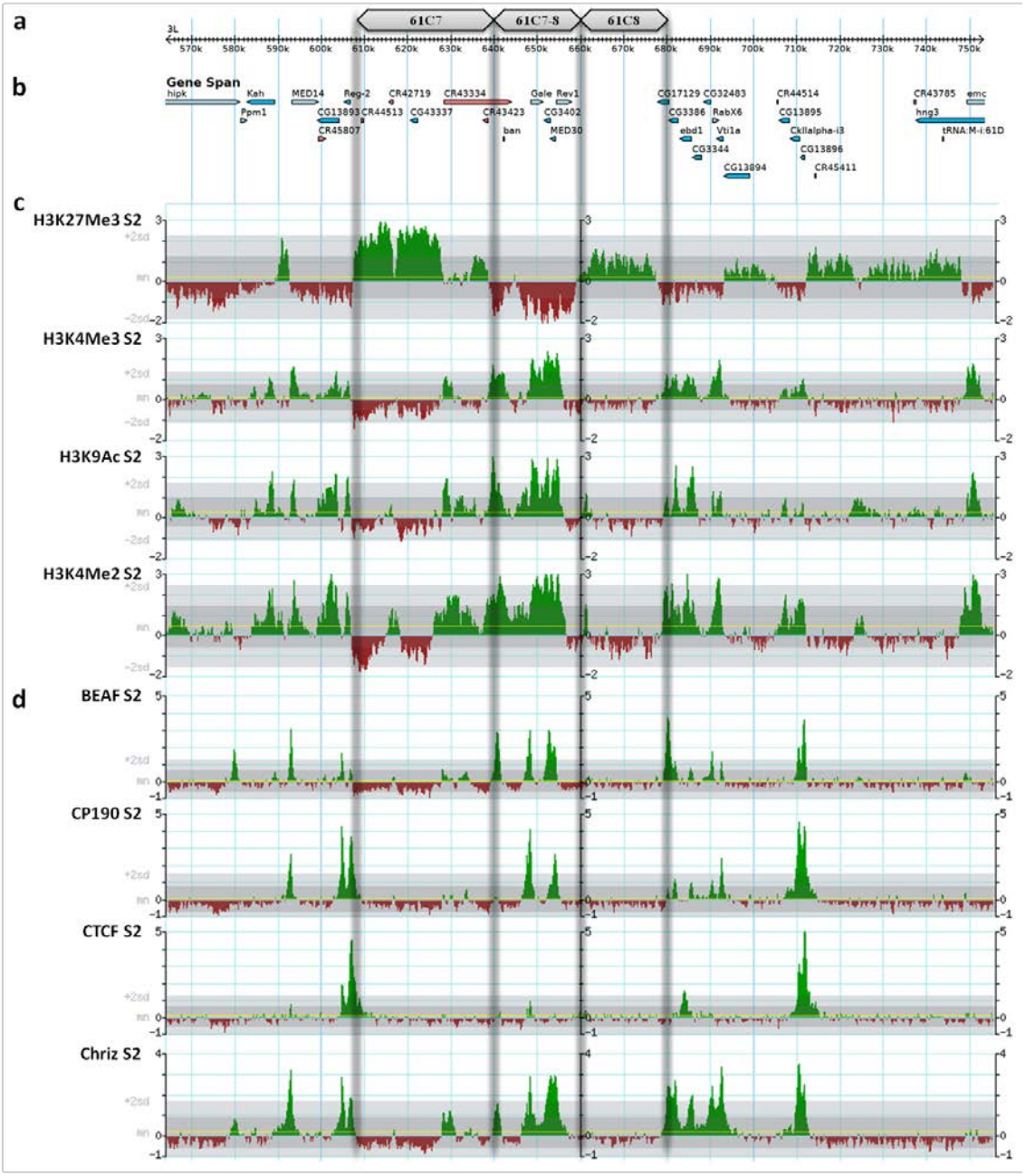

Online Resource 1: Chromatin profiles of the 61C7-61C8 region under investigation.

a) molecular coordinates of the chromosomal region under investigation b) Genes located in this region c) profiles of selected histone modifications mapped for this region for *Drosophila* S2-cells. From top to bottom: H3K27Me3, H3K4Me3, H3K9Ac, H3K4Me2; d) Similarly, profiles of selected chromatin proteins from top to bottom: BEAF-32, CP190, CTCF, Chriz. The semitransparent bars indicate the position of the domain boundaries mapped by our *in situ* approach.

Online Resource 2 (ESM2)

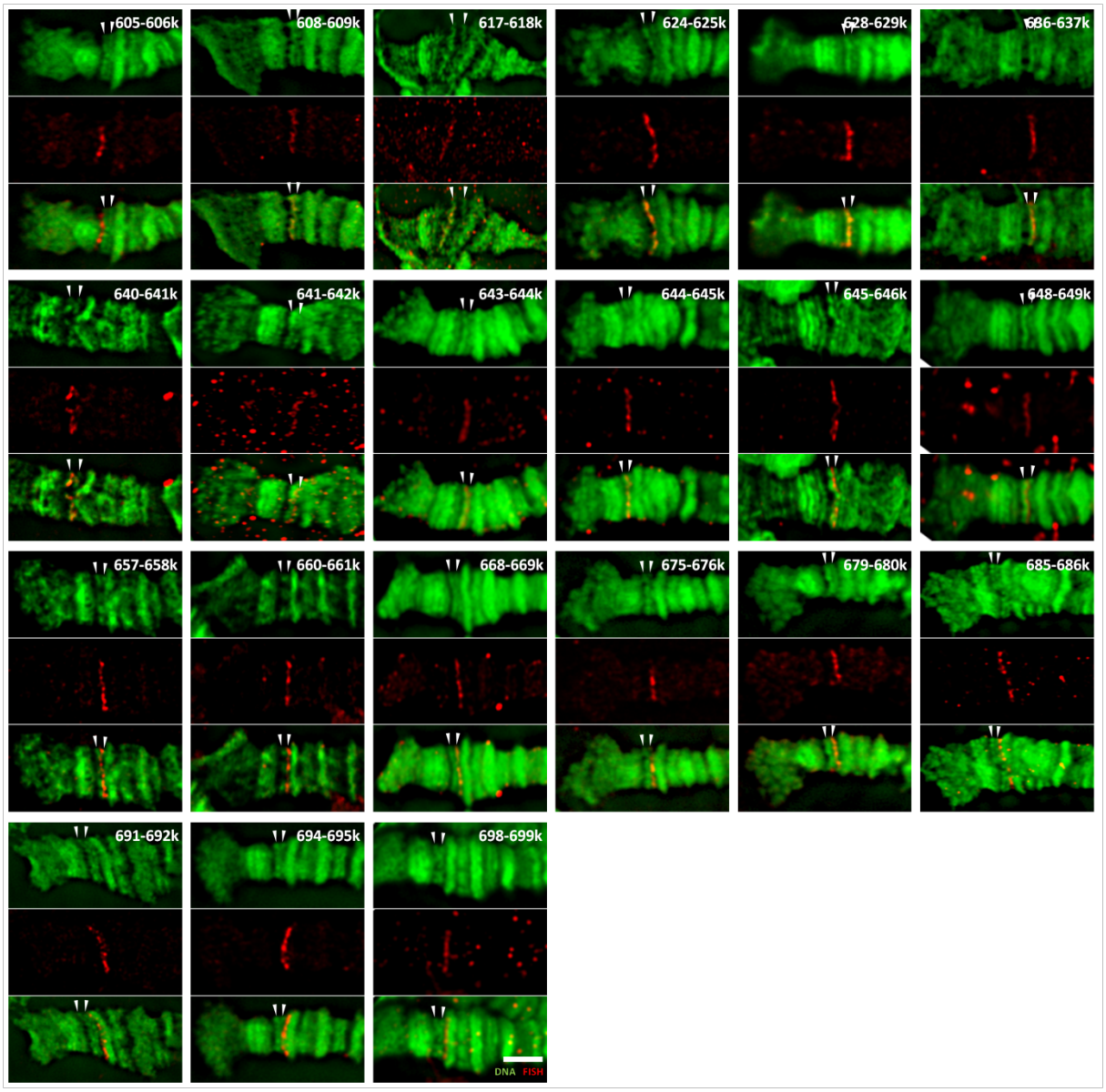

Online Resource 2: Representative images of all *in situ* hybridization probes mapped to the 61C7-8 region.

Panels show representative *in situ* hybridizations in the 3L: 61C7-8 region with all 1 kbp probes used from distal to proximal. The genomic coordinates of the probes indicated in the top image of each panel are as given in table 1. Top in each panel shows DNA staining (green), middle: *in situ* hybridization signal (red), bottom: merge. White arrowheads indicate the bands at 61C7 and 61C8 respectively. Distal is to the left. Bar at the bottom of last panel is 3 μm.

Online Resource 3 (ESM3)

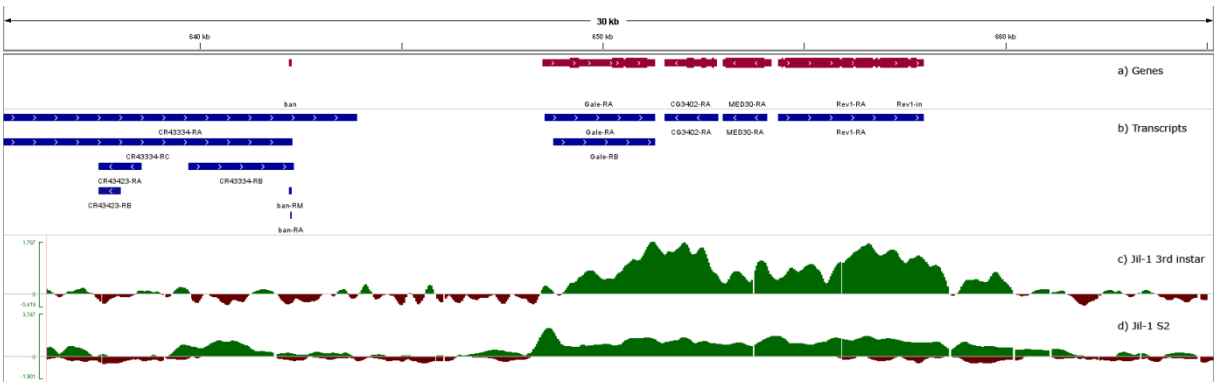

Online Resource 3: Jil-1 binding in the 61C7-8 open domain.

Figure shows profiles of Jil-1 binding in 30 kbp of 61C7-8 region. a) Genes located in the region; b) Transcripts located in the region; c) Jil-1 binding profile in 3rd instar larvae tissues (ChIP-chip dataset is available at modENCODE database (http://modencode.org/), submission [modENCODE_3292]); d) Jil-1 binding profile in S2 cells (ChIP-chip dataset is available at modENCODE database, submission [modENCODE_3038])

735 Online Resource 4 (ESM4)

736

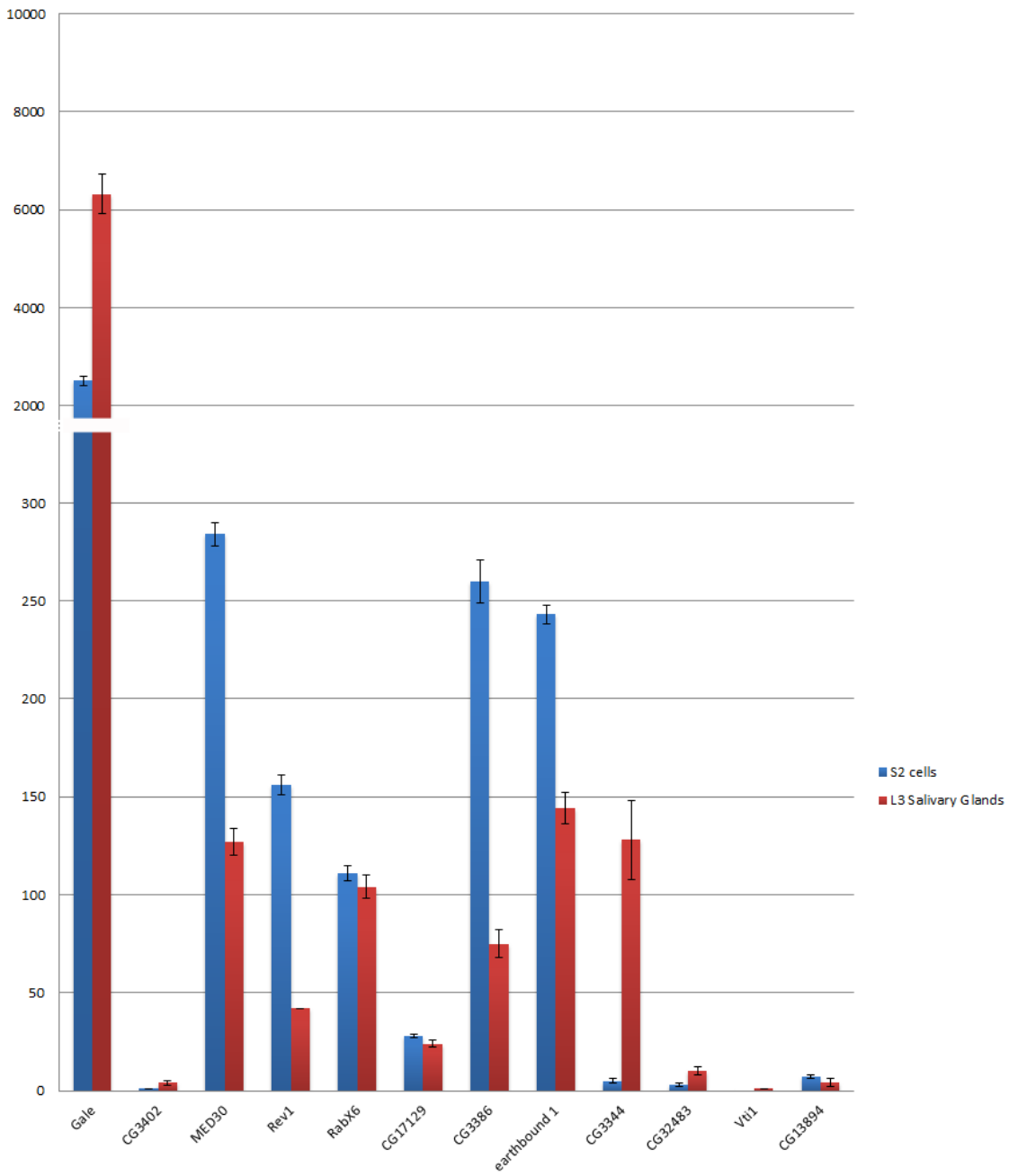

737

738 **Online Resource 4: Gene expression in 61C7-8 and the adjacent interband domain.**

739 Figure shows the expression levels of coding genes located in the 61C7-8 region as listed in S2 cells
740 (blue) and in 3rd instar larvae salivary glands (red). Data is available at FlyAtlas database
741 (http://www.flyatlas.org/).

742

743 Online Resource 5 (ESM5)

genomic coordinates of FISH-probes in kbp	normalized pixel distance of FISH signal to C7 reference band									arithmetic average and standard deviation
605-606	-2,5	-5,7	-7,1	-10	-7,5	-5,7				-6,42 ± 2,49
608-609	0	3,3	0	-2,5						0,21 ± 2,39
617-618	1,1	0	0	1,3						0,59 ± 0,68
624-625	0	2,2	1,1	0	2,5					0,83 ± 1,18
628-629	0	0	1,3	1,4	0,8					0,7 ± 0,68
636-637	1,3	-1,4	1,7	0	1,3	1,4				0,7 ± 1,19
640-641	1,8	1,3	0	0						0,77 ± 0,92
641-642	2	3,8	-1,4	1,4	1,4	3	0	0		1,37 ± 1,7
643-644	0	2,5	3,3	0	3,8					1,92 ± 1,81
644-645	3,3	1,7	1,7	2	2,9	2				2,26 ± 0,68
645-646	2	1,4	1,4	3,3	2,5	2,9	2	2,5	5	2,4 ± 1,11
648-649	5	2,9	2,9	5	3,3	2,9				3,65 ± 1,06
657-658	6,7	6,7	6	6						6,34 ± 0,39
660-661	10	13	8,3							10,28 ± 2,1
668-669	12	8,3	13							10,94 ± 2,28
675-676	12	12	12							11,83 ± 0,17
679-680	14	14	12	8						12 ± 2,83
685-686	20	14	23	23	14	16				18,36 ± 4,05
691-692	21	20	26	21						21,96 ± 2,55
694-695	20	30	18	22						22,58 ± 5,17
698-699	30	22	20							24 ± 5,29

744

745 **Online Resource 5: Table with data to obtain the relative distances of the *in situ* probes in 61C7-8**
746 (compare Fig 3)**.**